Photonic Clays: A New Family of Functional 1D Photonic Crystals

Bettina V. Lotsch and Geoffrey A. Ozin*

Chemistry Department, University of Toronto, 80 St. George Street, Toronto, Ontario, M5S 3H6 Canada

ABSTRACT Clays have shown potential as intelligent optical sensing platforms when integrated into a one-dimensional photonic crystal (PC) environment. The clay component imparts intrinsic functionality to the multilayer system by combining the signature ion exchange with the tunable structural color of photonic crystals, giving rise to environmentally sensitive photonic clay architectures. We have fabricated different Laponite-based 1D PCs and clay defect PCs by simple bottom-up self-assembly methodologies and elaborate their working principles and chemically encoded optical response. Accessibility of the multilayer system to analytes is studied on the background of the barrier properties of clays and diffusion control by the mesoporous oxide layers. The time dependence of analyte uptake and the extent and driving force for analyte release are pointed out and discussed in the context of different interactions between the clay layers and analytes. We demonstrate the possibility of optical cycling associated with repeated analyte uptake and removal processes, rendering photonic clays recyclable and low cost sensing platforms with simple optical read-out.

KEYWORDS: photonic crystal · clay · structural color · sensor · thin films

Chemically tailored photonic crystals (PCs) recently started to unfold their potential beyond their use as reflective coatings, mirrors, or lasing environments,[1−12] and the concept of structural color combined with advanced microfabrication strategies continues to set the stage for a new generation of functional optical materials.[13,14]

The first generation of 1D PCs has been extended recently to a class of environmentally sensitive PCs which provide tunability of the optical stop band as a result of physisorption of analytes within the multilayer architectures. To this end, 1D periodic PCs based on different ordered mesoporous, nanocrystalline, and layer-by-layer assembled thin films were designed.[15−21] As well, optical contrast was introduced into 1D PCs by porosity changes in a single material such as silicon.[22−25] To overcome the inherent limitations of this second generation of 1D PCs, imposed in part by the necessity for *in situ* sensing and a limited spectrum of gaseous and liquid analytes, layered materials which interact more strongly with a wide range of analytes are desirable. We have therefore suggested a third generation of 1D PCs based on the implementation of intrinsically active layered materials.[26] Thus, inherent functionality arises from a chemical response to external stimuli, which translates into a change in the optical thickness of the multilayer system and thus a shift in the photonic stop band. The novelty of this approach lies in the realization of label-free tunable structural color from inherently colorless materials, which when integrated into a PC environment translate chemical functionality into an optical read-out.

As we could demonstrate recently, inorganic clays gain luster by "throwing" them into a 1D periodic superlattice together with a high-index material such as titanium dioxide.[26] In this novel genre of "photonic clays", christened clay Bragg stacks (CBSs), the layered silicate acts as optical transducer of chemical processes such as intercalation, adsorption, and ion exchange, thereby enabling one to visualize for the first time "optically silent" processes occurring in the solid phase: According to the optical Bragg law, $\lambda_B = 2n_{eff}\Lambda$ (where n_{eff} is the effective refractive index of a bilayer, and Λ its period), changes in n_{eff} or in the clay layer dimension upon analyte adsorption directly translate into a shift of the optical stop band. The chemical signature of clay minerals embedded in a PC environment has great potential for use in intelligent optical sensing platforms featuring simple read-out and a wide range of applications due to its benign character and ease of fabrication.

In this work, we expand on the recently introduced concept of photonic clays by demonstrating the versatility of different clay-based photonic crystal architectures as

*Address correspondence to gozin@chem.utoronto.ca.

Received for review June 16, 2008 and accepted September 15, 2008.

Published online October 1, 2008.
10.1021/nn800375e CCC: $40.75

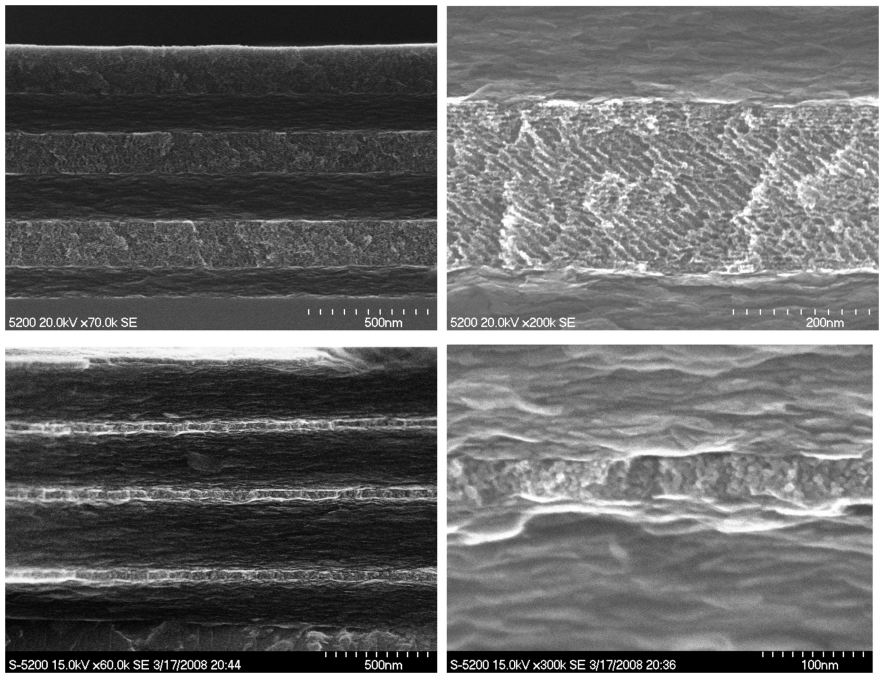

Figure 1. Top: SEM cross-section images of two three-bilayer Laponite-$mTiO_2$ BSs (160 ± 20 and 185 ± 30 nm (left), 270 ± 40 and 180 ± 30 nm for Laponite and $mTiO_2$, respectively (right)). Bottom: Four-bilayer Laponite-$NPTiO_2$ BSs (left), and magnification of the interface between the clay lamellae and nanoparticles (right). Layer thicknesses are 280 ± 40 nm (Laponite) and 44 ± 4 nm ($NPTiO_2$) (note that the thickness of the different clay layers in a CBS as well as the lateral thickness can vary up to 10−15% around the given average).

intelligent optical materials with both analyte uptake and release capabilities. We investigate the interplay between different chemical and physical processes leading to an optical response, as well as possible implications for the use of CBSs as optical sensing platforms. Gaining a better understanding of the underlying mechanism governing the interaction between the PC backbone and analytes is crucial not only for appraising the sensing performance of CBSs but also for evaluating the material profile necessary to create a new generation of tailor-made functional PCs.

RESULTS AND DISCUSSION

Clay Bragg Stack Architectures. CBSs were assembled with layers primarily based on the smectite clay Laponite (empirical formula $Na^{+}_{0.7}[(Si_8Mg_{5.5}Li_{0.3})O_{20}(OH)_4]^{-0.7}$) and titania to ensure sufficiently high refractive index contrast. Laponite can be fashioned into optically homogeneous thin films owing to its nanosized platelets which tend to lay on top of each other in a planar fashion, thereby forming smooth films with well-defined interfaces (Figure 1). To maintain a high level of accessibility of the entire multilayer system to analytes, both mesoporous and nanocrystalline titania were singled out as the most appropriate sources of titania. Mesoporous silica ($mSiO_2$) was used as an alternative to mesoporous titania ($mTiO_2$) to probe the effect of the mesopore structure on analyte diffusion and accessibility within the multilayer systems. Although the optical quality of the $mSiO_2$-based stacks is superior to that of $mTiO_2$-based ones, the reflectivities of the stop band in the former case are expectedly low due to the small refractive index contrast.

The layers are assembled step-by-step by spin-coating aqueous solutions of silica or titania sols, or titania nanoparticle suspension and Laponite, respectively, followed by calcination to remove the templates or binders used to enhance the film quality. Except for the defect Bragg stacks, which were constructed from a total of 14 mesoporous silica and titania layers, Bragg stacks made from three bilayers were used in all experiments. By varying concentration and spinning rate, the layer thicknesses of both clay and metal oxide can be tuned in a wide range, which together with good interface quality and film homogeneity allows for a judicious tunability of the position of the stop band and ensures high optical quality of the CBSs.[26]

As accessibility of the multilayer system to analytes is a crucial issue, we aimed at maximizing the porosity not only of the nonfunctional oxide but also of the clay

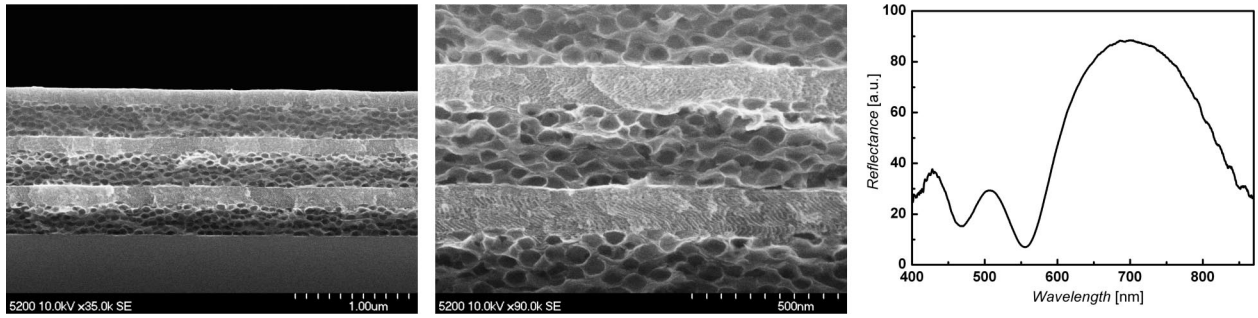

Figure 2. Cross-sectional view (left) and magnification (middle) of a three-bilayer CBS composed of porous clay layers (274 ± 40 nm) and $mTiO_2$ (150 ± 22 nm). Right: Optical spectrum of a porous CBS (90 ± 13 nm/150 ± 22 nm, Laponite/$mTiO_2$) with its stop band in the visible range, showing reflectance values in excess of 80%. The porosity of the Laponite layers is around 86%.

layers. To this end, we fabricated porous Laponite-mTiO$_2$ CBSs, the resulting multilayer structure featuring four hierarchy levels in terms of porosity and assembly length scales (micro, meso, ultrameso, and macro): Laponite layers with ultramesopores were fabricated by a hard-templating method based on sacrificial polystyrene templates, which are sandwiched between mesoporous titania to maintain a high refractive index contrast and maximize accessibility of the PC backbone to analytes (Figure 2).

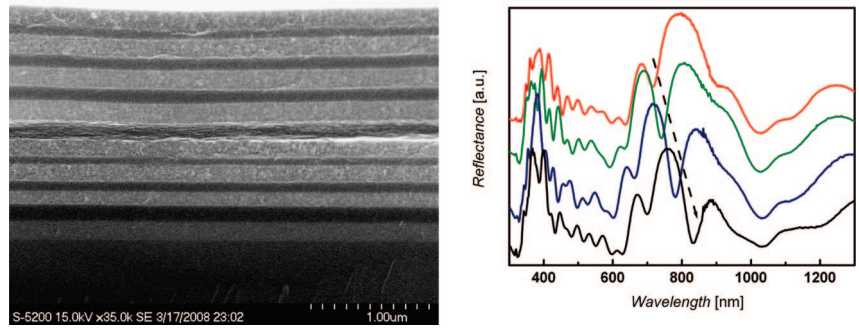

Figure 3. SEM cross-section image (left) of a planar clay defect 1D PC composed of a Laponite defect layer sandwiched between 7 + 7 mTiO$_2$/mSiO$_2$ layers with thicknesses of 130 ± 19 nm (mTiO$_2$) and 104 ± 15 nm (mSiO$_2$). Right: Corresponding UV−vis reflection spectra of defect PCs with linearly increasing thickness of the clay layer (≈120 to 400 nm, top to bottom).

Controlled tailoring of the PC architecture and its optical properties is further possible by introducing optical dopants or defects into the backbone of the PC. Building a planar defect into a multilayer structure disrupts its periodicity, thereby generating a small range of allowed frequencies within the photon density of states which gives rise to a so-called pass band, within the stop band of the 1D PC.[14,27] We have fashioned Laponite defect layers into a mesoporous silica−titania-based 1D PC as demonstrated in Figure 3. Varying the thickness of the clay defect translates into a shift of the transmission window superimposed on the stop band. Since the fwhm of the pass band is narrow compared to the stop band, defect stacks turn out to be particularly sensitive to environmental changes and, thus, may be suitable if high precision read-out in conjunction with small optical shifts is required.

Accessibility to Analytes. Clay is commonly known as a layered material capable of acting as a barrier material, for example, with respect to certain gases, and therefore the accessibility of the CBS multilayer system for analytes may be severely limited. To check whether permeability issues have to be taken into account, several bi- and multilayer systems were exposed to solutions of the cationic surfactant cetyltrimethylammonium bromide (CTAB) used in this work as a model analyte and subjected to elemental analysis. Table 1 outlines the C, N, and H contents observed for architectures of different size and succession of the layers. In particular, a significant discrepancy in the organics content is observed for the two scenarios where Laponite is either the top or the bottom layer. Where the bilayers start with Laponite as the bottom layer as typically used for the CBSs in this work, the C/N/H content is more then halved compared to the opposite scenario. Where Laponite constitutes the top layer, the organics content is largely in agreement with that of a single Laponite film. On the other hand, a CBS composed of three bilayers with Laponite forming the bottom layer exhibits a C/N/H content similar to that of one bilayer. While this suggests that the analytes penetrate not only the top layers but also the entire multilayer system, the mesoporous layers at the same time seem to strongly diminish the analyte flow into the Bragg stack, presumably owing to strong interactions between the mesopore surface hydroxyl groups and the cationic analyte. The fact that the bilayers with Laponite on top have similar C/N/H contents as a single Laponite film is rationalized with the assumption that the surfactant is not specifically adsorbed only on the Laponite slabs but also on the mesopore surfaces to a certain extent. On the basis of the somewhat simplified scenario (see below) that analyte−clay interactions are mainly driven by ion exchange of the sodium ions of pristine Laponite by the cationic surfactants, the elemental analysis data suggest that in all cases complete ion exchange does not occur but instead part of the sodium ions are retained, yielding exchange values less than the theoretical ion exchange capacity of Laponite (≈50 meq 100 g^{-1}).[28−30]

TABLE 1. C, H, and N Contents of Different 1D PC and Thin Film Compositions after Exposure to 0.03 M CTAB Solutions for 1−3 Days

composition	C/wt %	H/wt %	N/wt %
(Lap−mTiO$_2$)	5.6	1.8	0.5
(Lap−mSiO$_2$)	4.4	1.7	0.3
(Lap−mTiO$_2$)$_3$	4.3−6.9	0.9−1.5	0.2−0.3
Laponite thin film	10.4	2.6	0.6
(mTiO$_2$−Lap)	9.8	2.4	0.7
(mSiO$_2$−Lap)	10.7	2.6	0.7

To independently confirm that the clay layers do not suppress the analyte flow inside the PC, we exposed mSiO$_2$ as well as mTiO$_2$-based CBSs to a solution of Rhodamine 6G, a cationic dye which can interact with the negatively charged clay layers as well as with Si−O$^-$ or Ti−O$^-$ groups on the surface of the mesoporous oxide layers.[31−34] Probing the emission and hence the spatial distribution of the dye along the cross-section of the three bilayer CBSs, which were not exposed directly to the Rhodamine 6G solution, by means of confocal microscopy suggests that the dye is distributed across the entire multilayer system (Figure 4). Visibility of the single layers is enhanced by the shift

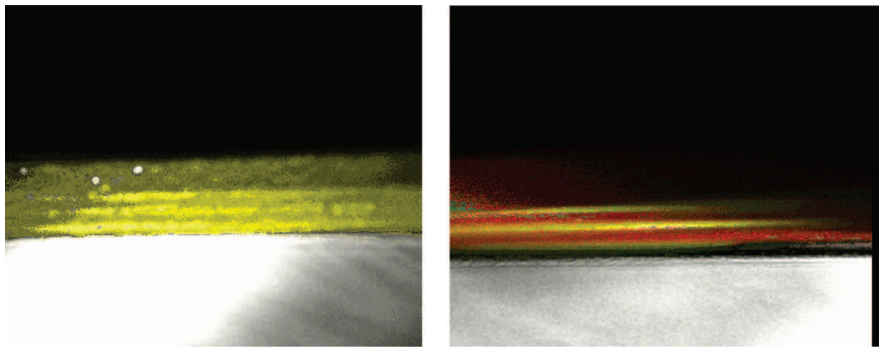

Figure 4. Cross-sectional laser confocal microscope images of Laponite−$mTiO_2$ (left) and Laponite−$mSiO_2$ (right) stacks covered with a micron-sized Laponite overlayer and soaked in Rhodamine 6G solution. Different emission wavelengths likely result from dye aggregation phenomena, giving rise to a shift in the emission wavelengths of the dyes in different host environments. Layer thicknesses are 440 ± 90 nm/300 ± 60 nm (Laponite/$mTiO_2$) and 350 ± 70 nm/300 ± 60 nm (Laponite/$mSiO_2$), and the clay overlayers are between 1 and 2 μm thick.

as well as intensity variations in the emission spectrum of Rhodamine 6G as a function of the environment of the dye molecules. Effects such as dye dimerization and aggregation or self-adsorption are commonly encountered phenomena that typically lead to a bathochromic shift of the fluorescence maximum of the dyes adsorbed on clays.[32,33] Although a thick (>1 μm) Laponite layer has been deposited on top of the PCs, the analyte possesses sufficient mobility to access the entire inner surface of the CBS. We therefore conclude that the dye, in spite of interacting with the oxide and clay layers, is able to either penetrate the entire multilayer system when entering from the top surface or else diffuses into the layers at the edges which are exposed to the solution.

An informative experiment associated with the optical response of 1D PCs containing a planar Laponite defect was carried out in order to probe the permeability of the mesoporous layers for analytes. As expected from the lower content of the "optically active" material, the shifts of both stop and pass bands after exposure to a CTAB solution are reduced compared to the Laponite−$mTiO_2$ architectures, yet still significant (Figure 5). In agreement with the expectations, the red shift of the pass band increases with increasing thickness of the clay defect, which also attests to the accessibility of the entire multilayer system to the cationic surfactant. Therefore, we conclude that, although the mesoporous oxide layers likely lead to a reduced equilibrium analyte flow through the 1D PC backbone, the accessibility of the latter is still fully retained.

Analyte Uptake and Release. Exposure of the CBSs to analyte solutions of different types leads to pronounced shifts of the stop band, which therefore acts as a probe of the clay−analyte interactions.[26] An important issue arising in this context is the nature of these interactions and especially as to whether ion exchange, intercalation, or simple adsorption processes trigger the optical response. Since Laponite possesses a specifically high external surface area due to the nanosized clay platelets (≈25 nm diameter, 1 nm height),[29,35] surface reactions are expected to gain importance over processes involving the clay interlayer space.

IR spectroscopy of various PC architectures and thin films qualitatively confirm the uptake of analytes, as can be seen by the presence of the ν(C−H) stretching vibrations around 2850 cm^{-1} and ν(C−N) at roughly 1400 cm^{-1} due to the quarternary ammonium cations and amines, which are absent in the original Bragg stacks (Figure 6, left). While this evidence suggests the presence of analytes within the 1D PC backbone after removal of the analyte solution and, therefore, the possibility of *ex situ* sensing, X-ray powder diffraction is a valuable tool to more specifically probe the nature of clay−analyte interactions. Although the broad 00*l* reflections of Laponite testify a rather pronounced stacking disorder and small crystallite sizes, the *d* spacing of Laponite clearly increases after exposure to different cationic analytes (Figure 6, right). This is in agreement with an at least partial intercalation of the surfactants into the intragallery space of Laponite, thereby prying open the clay layers. Although the shifts in *d* spacing are different for different analytes, they are relatively small compared to those observed for the same analytes and clays with a high layer charge density such as Montmorrilonite.[36−42] This may be rationalized by the assumption that, owing to the small layer charge density of Laponite,[43] the analytes take on a flat orientation in the interlayer space, corresponding to a monolayer of surfactants oriented with their molecular axis parallel to the layers. However, this does not exclude the possibility of the analytes being intercalated only to a cer-

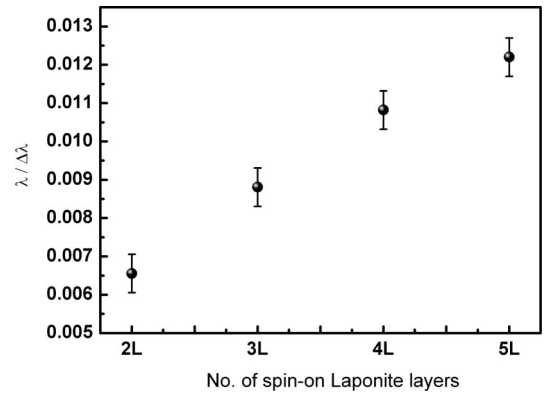

Figure 5. Red shift of the pass band of the Laponite defect PCs (UV−vis spectra shown in Figure 3, right) on exposure to a 0.03 M CTAB solution. The number of spin-coated Laponite layers is indicated as a measure for the increasing thickness of the defect; actual Laponite layer thicknesses vary between ≈120 and 400 nm.

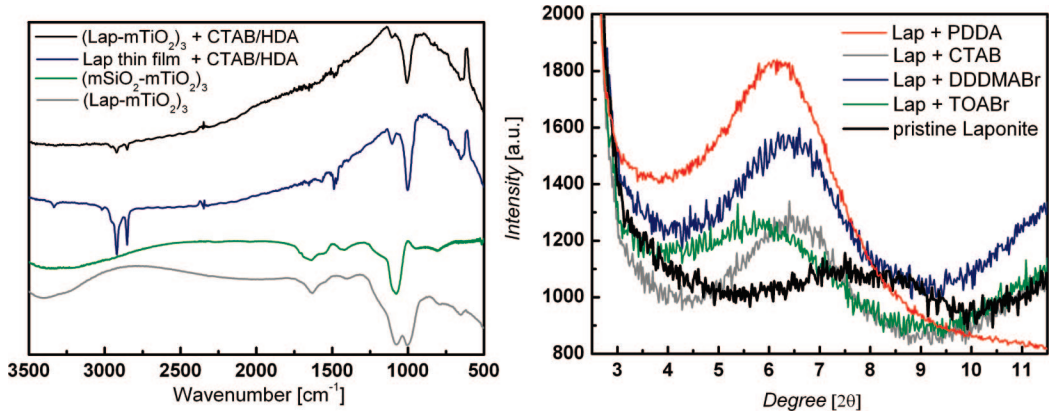

Figure 6. IR spectra (left) and X-ray powder patterns (right) of different 1D PC architectures and Laponite films before and after exposure to analytes (CTAB: cetyltrimethylammonium bromide; DDDMABr: didodecyldimethylammonium bromide; HDA: hexadecylamine; PDDA: poly(diallyldimethylammonium chloride); TOABr: tetraoctylammonium bromide).

tain extent, leading to a rather low intragallery loading fraction, while the rest is located on external adsorption sites on the clay surface.

Having confirmed that cationic analytes chemically interact with the clay layers, we now turn our focus to the time scale of this interaction and its dependence on the type of 1D PC backbone. We have already demonstrated that, for CTAB in an ethanol solution, analyte uptake proceeds within minutes as demonstrated by the evolution of the optical shift with time.[26] Taking the cationic polyelectrolyte poly(diallyldimethylammonium chloride), PDDA, as analyte in a water/ethanol solution, which according to Figure 6 (right) can intercalate between the clay sheets, we observe a similarly fast optical response irrespective of the type of 1D PC used.

As outlined in Figure 7, the time evolution of analyte uptake of the (Laponite−$mTiO_2$)$_3$ three-bilayer CBS closely resembles that of a pure Laponite thin film, yielding a saturation type growth curve and thus indicates that similar diffusion-based processes govern both uptake behaviors. However, the shifts are greater for Laponite than for the CBS, which is in agreement

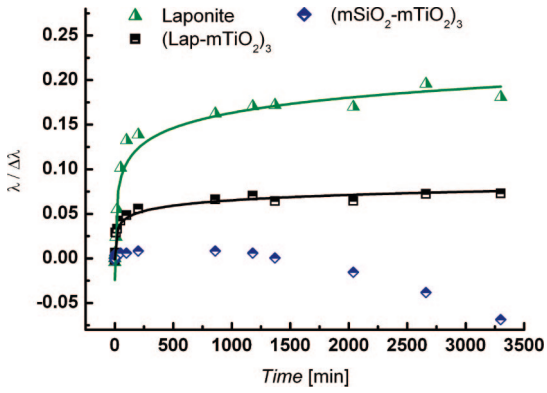

Figure 7. Uptake of PDDA by a Laponite thin film (≈400 nm), a three-bilayer Laponite−$mTiO_2$ Bragg stack (125 ± 19 nm/260 ± 40 nm (Laponite/$mTiO_2$)), and a three-bilayer mesoporous Bragg stack (220 ± 30 nm/260 ± 40 nm ($mSiO_2$/$mTiO_2$)), monitored by the shift of the stop band as a function of exposure time.

with the assumption based on elemental analysis data that the mesoporous layers reduce the total amount of analytes diffusing into the multilayer system.

In the early stages of analyte uptake, the ($mSiO_2$−$mTiO_2$)$_3$ Bragg stack shows an expectedly small red shift; however, after prolonged exposure (>1000 min), a reverse shift is observed, associated with changes of the shape of the optical spectra. This observation is in line with the onset of degradation of the mesoporous layers owing to their limited stability in the presence of water, which constitutes part of the analyte solution. Most likely, the instability is associated with the silica rather than with the titania component, as (Laponite−$mTiO_2$)$_3$ stacks do not show an analogous trend.

The rapid initial analyte uptake can best be rationalized with adsorption of the polyelectrolyte to the clay and mesopore surfaces, based on electrostatic interactions associated with partial ion exchange. However, as the exposure proceeds, a diffusion-based rearrangement of the clay−analyte interactions is likely to take place, leading in particular to migration of the adsorbents followed by a redistribution between the outer clay faces and the interlayer space as suggested by the X-ray diffraction measurements (Figure 6, right).[32]

Along similar lines, the question as to whether the analyte is reversibly or irreversibly attached to the clay and mesopore layers arises. To this end, we have studied the optical shifts of a three-bilayer (Laponite−$mTiO_2$)$_3$ CBS and Laponite thin film upon analyte exposure and subsequent soaking in ethanol for increasing periods of time. To probe the influence of the analyte structure on the reversibility of the clay−analyte interaction, we chose the linear chain surfactant CTAB and the branched TOABr (tetraoctylammonium bromide) as model systems (Figure 8). Notably, in both cases, leaking of the analytes into solution occurs, which was confirmed by IR spectroscopy (see Supporting Information) based on the diminishing C−H stretching vibration of the adsorbed analytes.

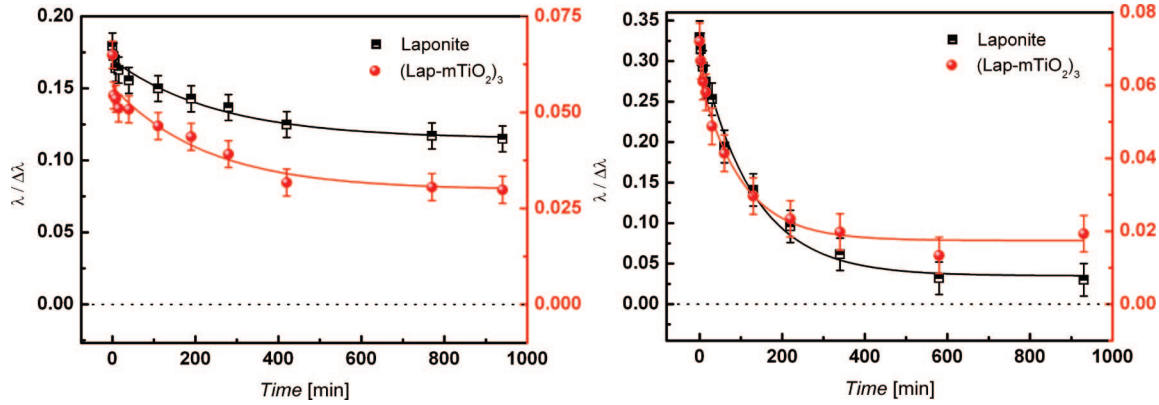

Figure 8. Release kinetics for CTAB (left) and TOABr (right) adsorbed on a Laponite thin film (≈400 nm) and a three-bilayer Laponite−$mTiO_2$ Bragg stack (230 ± 34 nm/140 ± 30 nm (Laponite/$mTiO_2$)), measured by the relative shift of the stop band as a function of exposure to pure EtOH solution. The dotted line corresponds to complete release of the analyte.

Comparing the release kinetics of both surfactants, that of CTAB occurs on a slower time scale compared to that of TOABr, yet both of them give rise to an approximately exponential decrease in the shift of the stop band, which levels off after several hours. A second noticeable detail is that in both cases the final equilibrium shift does not correspond to the initial one prior to analyte uptake, suggesting that the release is not complete in both cases. However, it is much more pronounced for TOABr than for CTAB both for the Laponite thin film and the CBS. In terms of a distinction between these two systems, the CTAB leakage seems to be relatively more pronounced for the CBS compared to the Laponite film, whereas the reverse scenario holds for TOABr. This may be rationalized with a relatively stronger retention of TOABr in the mesopores due to stronger interaction with the pore walls or impeded diffusion of the bulkier surfactant back out of the multilayer system into solution. On the other hand, the strong overall blue shift observed for TOABr compared to CTAB points to a difference in the nature of the interactions between the two analytes and the PC backbone. We assume that the bulky TOABr is primarily adsorbed on the outer clay faces owing to frustrated intercalation,[44] and hence more mobile, making it more prone to being washed out by the soaking solution than the linear chain and less bulky surfactant CTAB. The fact that at least partial analyte leakage occurs in both cases, however, is not in agreement with the assumption of ion exchange intercalation of the surfactant and replacement of sodium ions by the latter as the only clay−analyte interaction mode. If ion exchange was the major type of interaction between analyte and clay, leakage is unlikely to occur owing to the violation of charge balance considerations. Electro-neutrality can, however, be retained upon analyte release if we assume two alternative interaction pathways: The surfactants may not only be intercalated as cations, thereby replacing the sodium ions that compensate the anionic layer charge, but also in a neutral state, that is, as ion pairs, a phenomenon we term co-intercalation. This process is triggered if the charge density of the clay layers is small, resulting in a lower packing density of the guest species, and if the interactions between the guest species or between the guest species and the initial interlayer cations. As a result, uptake of excess guest species may occur, which are not required for charge compensation, but can additionally be accommodated in the intragallery space. Alternatively, adsorption of the cationic surfactants and their counteranions may occur by housing the neutral species in the electrostatic double layer around the clay surface. In particular, the edges of Laponite bear a slightly positive charge,[29] which facilitates the adsorption of anions along with the cations adsorbed to the negatively charged clay faces.

Taking all three interaction mechanisms outlined in Scheme 1 into account, the fact that release of analytes is observed is in line with a combination of ion exchange on the one hand and co-intercalation or ion pair adsorption on the other hand as analyte uptake mechanisms. Thus, the leakage of loosely adsorbed or co-intercalated species gives rise to the gradual blue shift observed upon soaking in ethanol solution, whereas the final equilibrium red shift of the stop band is due to the permanently exchanged surfactant cat-

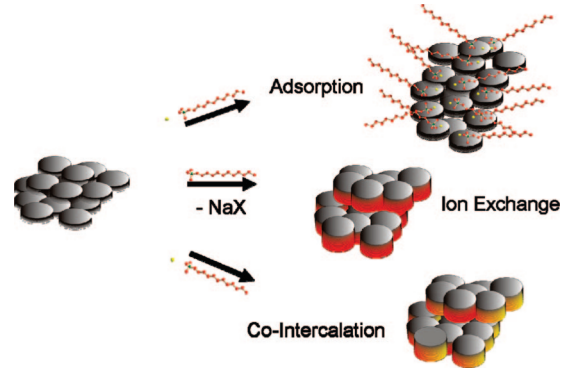

Scheme 1. Proposed modes of interaction between clay platelets and surfactant salts. A combination of all three mechanisms is likely to operate in the case of Laponite, and migration of the analytes between the outer and inner surfaces of the clay may also occur.

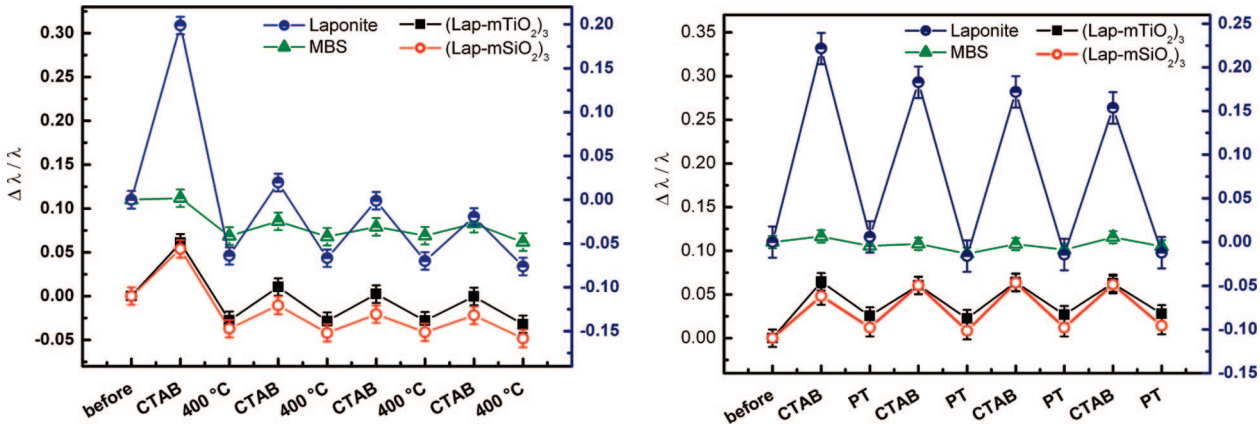

Figure 9. Left: Optical shift following repeated calcination (400 °C) and CTAB uptake cycles. Right: Shifts after repeated plasma treatment and CTAB uptake cycles. Layer thicknesses are ≈500 nm (Laponite), 250 ± 37 nm/140 ± 20 nm (Laponite/$mTiO_2$), 225 ± 33 nm/220 ± 30 nm (Laponite/$mSiO_2$), 220 ± 30 nm/140 ± 20 nm ($mSiO_2$/$mTiO_2$).

ions. Thus, the difference in the extent of analyte leakage for CTAB and TOABr may be traced back to a more adsorption-based interaction for the latter due to frustrated intercalation in contrast to a higher extent of intercalation with ion exchange in the case of the less bulky CTAB.

Optical Cycling. The usefulness of CBSs as optical sensing devices is crucially dependent on the feasibility to "recycle" the clay 1D PC for repeated sensing of analytes. This requires both mechanical stability of the 1D PC backbone, namely, sufficient adhesion between the layers and between the multilayer system and substrate, and the possibility to regenerate the optically active layer material and thus re-establish its sensitivity after saturation with analytes.

We have addressed this issue by subjecting both $(Laponite-mTiO_2)_3$ and $(Laponite-mSiO_2)_3$ 1D PCs as well as a thin Laponite film and a three-bilayer mesoporous 1D PC for comparison to cycles of different treatments aimed at analyte exposure and subsequent removal. The harshest method of analyte removal involves repeated calcinations of the CBS after loading with CTAB. As pointed out in Figure 9 (left), the optical shifts observed for all 1D PCs during the process are similar, with the Laponite thin film and the Laponite-based 1D PCs expectedly showing the largest optical shift range. Upon calcination, the previous red shift after analyte exposure is reversed and a strong blue shift is observed, which probably is due to both reduction of the organic content and contraction of the 1D PC backbone. After calcination at 400 °C for 3 h, an exponential decrease in the shifts after repeated CTAB uptake is observed, pointing to a gradual degradation of the ion exchange and adsorption capacity of the CBS and Laponite film. This is due to a decreasing number of ion exchange sites, which are not regenerated but most likely charge compensated by protonation or else lost by framework condensation processes. Calcinations at 350 and 300 °C feature similar results (see Supporting Information); however, the treatment at 300 °C does not completely remove the analytes, judging from the slightly increasing red shift of the stop band after each thermal treatment with respect to the first calcination cycle. The contraction of the 1D PC backbone after thermal treatment, including partial crystallization of the mesoporous oxide and dehydration of the clay layers, reduces the swelling capability of Laponite and its accessibility to analytes, which further adds to the significantly reduced uptake ability after calcination. A qualitatively similar, yet less pronounced behavior is expected after treatment of the 1D PCs and Laponite thin film with an air plasma for more than 24 h to remove the organics from the 1D PC backbone (Figure 9, right). Whereas the optical shifts of the Laponite thin film gradually decrease, the CBSs do not show a very pronounced tendency toward saturation of their analyte sensing capability, but rather a relatively homogeneous reversible cycling behavior. However, the optical shifts of the CBSs after plasma treatment deviate slightly from their initial value before analyte exposure, which may be rationalized by an incomplete analyte removal and accumulation of analytes or their decomposition products within the active layers. Therefore, we assume that after prolonged cycling, the number of available ion exchange and adsorption sites gradually diminishes, leading finally to a decrease in the optical response of the CBSs.

An alternative and rather soft regeneration method is the exposure of the CBSs to a NaCl solution to exchange the cationic analytes by sodium ions and, thus, to re-establish the sodium form of the Laponite layers. This process is demonstrated for a $(Laponite-mTiO_2)_3$ CBS and a Laponite thin film in Figure 10. To monitor the concomitant analyte loading and removal process, IR spectra of the samples were taken after each step (Figure 10, right). Both systems show a periodic optical response to repeated CTAB loading and unloading cycles, with the optical shifts being larger than in the two alternative treatments outlined above. This is mainly a consequence of the use of ethanol−water

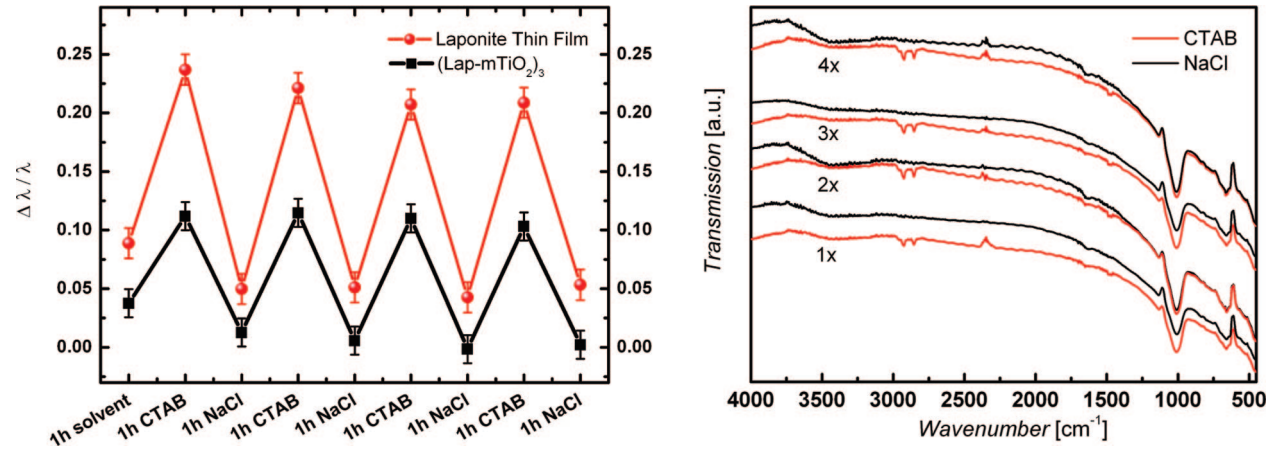

Figure 10. Relative optical shifts (left) of the stop band on repeated CTAB deintercalation with NaCl solution and (right) associated IR spectra of the Laponite−mTiO$_2$ CBS. Layer thicknesses are ≈500 nm (Laponite) and 250 ± 37 nm/140 ± 20 nm (Laponite/mTiO$_2$).

mixtures as a solvent, which enhance the solubility of NaCl and at the same time increase the swelling capability and, thus, accessibility of the clay layers. Whereas the relative optical shifts of the Laponite film after CTAB loading slightly decrease on repeated cycling, which is presumably due to the limited stability of Laponite films in the presence of water, the CBS exhibits a good cycling performance. The concomitant optical switching is also clearly mirrored by the appearance and disappearance of the C−H stretching mode of the analytes in the IR spectra. We therefore conclude that the solution de-intercalation treatment is the most efficient and a largely reversible means of "optical cycling" and bodes well for the use of CBSs as "recyclable" chemo-optical sensors.

CONCLUSIONS

In the above study, we have designed, optimized, and comprehensively characterized a novel family of clay-based 1D photonic crystal architectures christened clay Bragg stacks. The Laponite−clay interactions are manifold, and the sensing event can be traced back to interplay of ion exchange, intercalation, and adsorption processes involving the entire multilayer system, with the clay layers clearly representing the major functional component. Accessibility of the entire multilayer system is ensured in spite of the barrier properties of clay and the pronounced "protection" of the Laponite layers by the mesoporous oxide layers. The optically encoded uptake of PDDA exhibits a saturation type behavior and suggests rapid analyte uptake kinetics. Extent and time evolution of analyte release could be correlated with the nature of the surfactant, and different models for clay−analyte interactions were put forward. Recycling of the clay PCs and use in multiple sensing events was demonstrated by regenerating the CBSs on exposure to NaCl solution, which adds a valuable feature and holds promise for the use of photonic clays as environmentally friendly, easy to handle optical sensing platforms. By exploiting the optical fingerprints of CBS, namely, accessibility to various analytes and tunable analyte release, photonic clays may be developed into *active* sensing materials based on the coupling of the optical response with a specific function, such as drug release, detoxification, or antimicrobial activity, which is actively being investigated in our laboratory. In conclusion, the unique versatility of clays, possibly combined with that of another active layer material, lends itself well as the starting basis for the creation of a whole new generation of tunable, intrinsically functional photonic crystal sensors.

METHODS

Materials. Cetyltrimethylammonium bromide (95%), ethanol (anhydrous, denatured), poly(diallyldimethylammonium chloride) (98%), tetraethyl orthosilicate (TEOS, 98%), and titanium(IV) ethoxide (Ti(OEt)$_4$, Ti ~20% in ethanol, techn.) were purchased from Sigma-Aldrich; 1-butanol (>99.4%) was supplied by ACP, and concentrated HCl was obtained from Fisher. The nonionic triblock copolymers Pluronic P123 ((EO)$_{20}$(PO)$_{70}$(EO)$_{20}$, average molecular weight 8500 g · mol^{-1}) and F127 ((EO)$_{100}$(PO)$_{70}$(EO)$_{100}$, average molecular weight 12 600 g · mol^{-1}, BASF) were utilized as structure-directing agents in the synthesis of mesoporous TiO$_2$ and SiO$_2$, respectively. All chemicals were used as received. Films were deposited on Si wafers supplied by Wafer World.

Syntheses. Transparent suspensions of Laponite RD (SYnL-1, Southern Clay Products, and The Clay Minerals Society Inc. RD) were obtained by dispersing the clay in water (0.18−0.30 g, 10 mL of H$_2$O) under vigorous stirring for 5 h. Typically, a 3 wt % suspension of clay was filtered (0.2 μm) and spun on a Si wafer cleaned with Piranha solution (H$_2$SO$_4$/H$_2$O$_2$ 3:1) and treated with an air plasma for at least 15 min to increase the hydrophilicity and, thus, wettability of the surface. To vary the thickness of the Laponite layer between 50 and 600 nm, multiple spin-coating cycles at 2500 rpm for ≈1−2 min were performed. Titania nanoparticles (diameter ≈ 5 nm) were synthesized under hydrothermal conditions by adding dropwise at room temperature Ti(OEt)$_4$ (6.25 mL) to 0.1 M HNO$_3$ (37.5 mL) under stirring and heating the mixture at 80 °C for 8 h. To improve the film quality, 2.5 wt % of polyethylene glycol (M_w = 8000 g/mol) was added for spin-

coating (3000 rpm, 60s). The films were calcined at 200 °C for 1 h. The syntheses of the mesoporous oxides $mSiO_2$ and $mTiO_2$ were carried out according to a procedure described in a previous report.[15,26] Briefly, the $mSiO_2$ sol was prepared based on a mixture of TEOS (2.08 g), F127 (1.0 g), HCl (2 M, 0.1 g), ethanol (10.0 g), and deionized water (0.9 g) and stirred at room temperature for 3 h. The synthesis mixture of $mTiO_2$ was composed of $Ti(OEt)_4$ (2.10 g), concentrated HCl (1.35 mL), P123 (0.65 g), and BuOH (6 g) and aged for 3 h prior to spin-coating at 5000 rpm for 20 s. Multiple Laponite−mesoporous oxide bilayer architectures were fabricated by alternately spin-coating Laponite and the respective sol, including film aging (1 day 20 °C/80% RH) and calcination (300−350 °C, 1.5 h, heating rate 1 °C min^{-1}) after addition of each mesoporous oxide layer for surfactant removal. Porous Laponite films were fabricated by spin-coating a suspension of Laponite and polystyrene spheres (3/5% w/w) at 2500 rpm for 1−2 min and removing the templates by calcination in air (350 °C, 2 h).

Optical Sensing Experiments. Prior to each experiment, three to four spots on a Si wafer were characterized by their micrograph image and the associated UV−vis spectrum. For 1D PCs with their stop band in the IR, we used the positions of a higher order band or characteristic fringes as reference. For identification of the optical shift in the UV−vis spectrum, the wafer was positioned on the optical stage by identifying the respective spots by their micrograph images.

Typical *ex situ* analyte uptake/sensing experiments were conducted by immersing the 1D PC on a Si wafer into an ethanol or ethanol/water solution (83.3/16.7% v/v) of the respective analyte (0.03−0.3 M) held at 60 °C under stirring for the required period of time (1 h to 3 days). After immersion, the wafers were removed and rinsed with EtOH and then immersed in ethanol (10 mL) for 10 min, with the washing solution being changed once, and dried in a stream of nitrogen. For the optical cycling experiments, the samples were alternately exposed to 0.03 M solutions of CTAB in ethanol for 15 h and thermal (3 h at 400 °C, 1 °C min^{-1}) or plasma treatment (24−32 h, air plasma). De-intercalation studies were carried out by alternately exposing the CBSs to 0.1 M solutions of CTAB and NaCl in water/ethanol mixtures (33/77% v/v) at 60 °C for 1 h, respectively. In the analyte release studies, wafers were soaked in the analyte solutions (0.03 M, 30 mL of EtOH, 60 °C, 15 h) and rinsed with EtOH. Release was followed by immersion of the wafers in ethanol (30 mL) for various periods of time at room temperature. Sample preparation for confocal microscope imaging was done by fabricating CBSs with particularly thick (≥400 nm) Laponite and mesoporous oxide layers for resolution purposes by multiple spin-coating cycles and exposing the samples to a Rhodamine 6G solution (0.003 M in EtOH) for 2−30 h at 60 °C.

Characterization. Reflectance spectra in the range of 350 to 850 nm were collected using an Ocean Optics SD2000 fiber-optic diode-array dual-channel spectrometer interfaced with an Olympus BX41 binocular microscope by fiber optics, using the microscope's light source (Olympus TH4-100) and a 20X working distance objective (Olympus 20X/0.40 BD LMPlan FI). Reflectance spectra between 250 and 1500 nm were recorded using a Perkin-Elmer Lambda 900 UV−vis spectrometer. Confocal microscopy was performed on a Leica DMR microscope using 50X working distance objective lenses. To obtain cross-section images, the Si wafers were broken and placed in a SEM cross-section holder with the part not directly in contact with the dye solution during soaking facing upward. For excitation of the adsorbed Rhodamine 6G molecules, typically the 488 nm line of an Ar ion laser or, alternatively, the HeNe line at 543 nm was used. HRSEM was performed using a Hitachi S-5200 (10−15 kV, 15 mA). Wide-angle XRD patterns were obtained on a Scintag XDS 2000 diffractometer (Cu Kα radiation, 45 kV/40 mA) in θ−θ geometry. IR spectra were obtained on a Bruker Spektrum One (2000) FTIR spectrometer in transmission mode with the 1D PCs deposited on Si wafers.

Acknowledgment. G.A.O. is Government of Canada Research Chair in Materials Chemistry. The authors thank NSERC and the University of Toronto for financial support. We are grateful to Ilya Gourevich, Center for Nanostructure Imaging at the Department of Chemistry, University of Toronto, for his assistance with the confocal microscope imaging. We thank T. Bein for providing access to his X-ray facility at the Department of Chemistry, Ludwig-Maximilians-University of Munich, Germany. Funding granted by the Alexander von Humboldt foundation (Feodor-Lynen Postdoc scholarship for B.V.L.) is gratefully acknowledged.

Supporting Information Available: FTIR spectra during analyte release, optical cycling studies at 300−350 °C. This material is available free of charge *via* the Internet at http://pubs.acs.org.

REFERENCES AND NOTES

1. Arsenault, A.; Fournier-Bidoz, S.; Hatton, B.; Míguez, H.; Tetreault, N.; Vekris, E.; Wong, S.; Ming Yang, S.; Kitaev, V.; Ozin, G. A. Towards the Synthetic All-Optical Computer: Science Fiction or Reality. *J. Mater. Chem.* **2004**, *14*, 781–794.
2. Busch, K.; John, S. Photonic Band Gap Formation in Certain Self-Organizing Systems. *Phys. Rev. E* **1998**, *58*, 3896–3908.
3. Joannopoulos, J. D.; Villeneuve, P. R.; Fan, S. Photonic Crystals: Putting a New Twist on Light. *Nature* **1997**, *386*, 143–149.
4. Yablonovitch, E. Inhibited Spontaneous Emission in Solid-State Physics and Electronics. *Phys. Rev. Lett.* **1987**, *58*, 2059–2062.
5. John, S. Photonic Band Gap Formation in Certain Self-Organizing Systems. *Phys. Rev. Lett.* **1987**, *58*, 2486–2489.
6. Blanco, A.; Chomski, E.; Grabtchak, S.; Ibisate, M.; John, S.; Leonard, S. W.; Lopez, C.; Meseguer, F.; Míguez, H.; Mondia, J. P.; *et al.* Large-Scale Synthesis of a Silicon Photonic Crystal with a Complete 3-Dimensional Bandgap near 1.5 Micrometres. *Nature* **2000**, *405*, 437−440.
7. Xia, Y.; Gates, B.; Li, Z.-Y. Self-Assembly Approaches to Three-Dimensional Photonic Crystals. *Adv. Mater.* **2001**, *13*, 409–413.
8. Fernández, S.; Naranjo, F. B.; Calle, F.; Sánchez-García, M. A.; Calleja, E.; Vennéguès, P. High-Quality Distributed Bragg Reflectors for Resonant-Cavity Light-Emitting Diode Applications. *Phys. Status Solidi A* **2002**, *192*, 389–393.
9. Nakada, N.; Nakaji, M.; Ishikawa, H.; Egawa, T.; Umeno, M.; Jimbo, T. Improved Characteristics of InGaN Multiple-Quantum-Well Light-Emitting Diode by GaN/AlGaN Distributed Bragg Reflector Grown on Sapphire. *Appl. Phys. Lett.* **2000**, *76*, 1804–1806.
10. Someya, T.; Tachibana, K.; Lee, J.; Kamiya, T.; Arakawa, Y. Lasing Emission from an $In_{0.1}Ga_{0.9}N$ Vertical Cavity Surface Emitting Laser. *Jpn. J. Appl. Phys.* **1998**, *37*, L1424–L1426.
11. Grey, R.; Mansoor, F.; Haywood, S. K.; Hill, G.; Manson, N. J.; Walker, P. J. Growth of GaSb on GaAs/AlAs Mirrors for 1.68 μm Detectors. *Opt. Mater.* **1996**, *6*, 69–74.
12. Chen, L.; Towe, E. Photonic Band Gaps in Nanowire Superlattices. *Appl. Phys. Lett.* **2005**, *87*, 103111-1–103111-3.
13. Scott, R. W. J.; Yang, S. M.; Chabanis, G.; Coombs, N.; Williams, D. E.; Ozin, G. A. Tin Dioxide Opals and Inverted Opals. Near-Ideal Microstructures for Gas Sensors. *Adv. Mater.* **2001**, *13*, 1468–1472.
14. Arsenault, A.; Fleischhaker, F.; von Freymann, G.; Kitaev, V.; Miguez, H.; Mihi, A.; Tetreault, N.; Vekris, E.; Manners, I.; Aitchison, S.; *et al.* Perfecting Imperfection—Designer Defects in Colloidal Photonic Crystals. *Adv. Mater.* **2006**, *18*, 2779−2785.
15. Choi, S. Y.; Mamak, M.; von Freymann, G.; Chopra, N.; Ozin, G. A. Mesoporous Bragg Reflector Color Tunable Sensors. *Nano Lett.* **2006**, *6*, 2456–2461.
16. Fuertes, M. C.; López-; Alcaraz, F. J.; Marchi, M. C.; Troiani, H. E.; Luca, V.; Míguez, H.; Soler-Illia, G. J. de A. A. Photonic Crystals from Ordered Mesoporous Thin-Film Functional Building Blocks. *Adv. Funct. Mater.* **2007**, *17*, 1247–1254.
17. Lee, D.; Rubner, M. F.; Cohen, R. E. All-Nanoparticle Thin-Film Coatings. *Nano Lett.* **2006**, *6*, 2305–2312.
18. Wu, Z.; Lee, D.; Rubner, M. F.; Cohen, R. E. Structural Color in Porous, Superhydrophilic, and Self-Cleaning SiO_2/TiO_2 Bragg Stacks. *Small* **2007**, *3*, 1445–1451.

19. Lee, D.; Omolade, L. D.; Cohen, R. E.; Rubner, M. F. pH-Dependent Structure and Properties of TiO_2/SiO_2 Nanoparticle Multilayer Thin Films. *Chem. Mater.* **2007**, *19*, 1427–1433.
20. Fuertes, M. C.; Colodrero, S.; Lozano, G.; González-Elipe, A. R.; Grosso, D.; Boissière, C.; Sánchez, C.; Soler-Illia, G. J. de A. A.; Míguez, H. Sorption Properties of Mesoporous Multilayer Thin Films. *J. Phys. Chem. C* **2008**, *112*, 3157–3163.
21. Colodrero, S.; Ocana, M.; Míguez, H. Nanoparticle-Based One-Dimensional Photonic Crystals. *Langmuir* **2008**, *24*, 4430–4434.
22. Li, Y. Y.; Cunin, F.; Link, J. R.; Gao, T.; Betts, R. E.; Reiver, S. H.; Chin, V.; Bhatia, S. N.; Sailor, M. J. Polymer Replicas of Photonic Porous Silicon for Sensing and Drug Delivery Applications. *Science* **2003**, *229*, 2045–2047.
23. Zhai, L.; Nolte, A. J.; Cohen, R. E.; Rubner, M. F. pH-Gated Porosity Transitions of Polyelectrolyte Multilayers in Confined Geometries and their Application as Tunable Bragg Reflectors. *Macromolecules* **2004**, *37*, 6113–6123.
24. Sailor, M. J.; Link, J. R. "Smart Dust": Nanostructured Devices in a Grain of Sand. *Chem. Commun.* **2005**, 1375–1383.
25. King, B. H.; Ruminski, A. M.; Snyder, J. L.; Sailor, M. J. Optical-Fiber-Mounted Porous Silicon Photonic Crystals for Sensing Organic Vapor Breakthrough in Activated Carbon. *Adv. Mater.* **2007**, *19*, 4530–4534.
26. Lotsch, B. V.; Ozin; G. A. Clay Bragg Stack Optical Sensors. *Adv. Mater.* **2008**, in press.
27. Braun, P. V.; Rinne, S. A.; Garcia-Santamaria, F. Introducing Defects in 3D Photonic Crystals: State of the Art. *Adv. Mater.* **2006**, *18*, 2665–2678.
28. Borden, D.; Giese, R. F. Baseline Studies of the Clay Minerals Society Source Clays: Cation Exchange Capacity Measurements by the Ammonia-Electrode Method. *Clays Clay Min.* **2001**, *49*, 444–445.
29. *Laponite Brochure*; Southern Clay Products, Inc./Rockwood Additives Ltd., http://www.laponite.com.
30. Note that an accurate calculation of the theoretical amount of analyte adsorbed on the multilayer system is complicated by the following unknown quantities: relative amounts of oxide *versus* clay (including porosity of the meso layers), hydration state of the clay layers, adsorption mechanisms: ion exchange, co-intercalation, adsorption of neutral salts.
31. Arbeloa, F. L.; Martínez, V. M.; López, T. A.; Arbeloa, T.; Arbeloa, I. L. Photoresponse and Anisotropy of Rhodamine Dye Intercalated in Ordered Clay Layered Films. *J. Photochem. Photobiol. C: Photochem. Rev.* **2007**, *8*, 85–108.
32. Gemeay, A. H. Adsorption Characteristics and the Kinetics of the Cation Exchange of Rhodamine-6G with Na^+-Montmorillonite. *J. Colloid Interface Sci.* **2002**, *251*, 235–241.
33. López Arbeloa, F.; López Arbeloa, T.; López Arbeloa, I. Spectroscopy of Rhodamine 6G Adsorbed on Sepiolite Aqueous Suspensions. *J. Colloid Interface Sci.* **1997**, *187*, 105–112.
34. Tapia, M. J.; López Arbeloa, F.; López Arbeloa, T.; López Arbeloa, I.; Schoonheydt, R. A. Spectroscopic Study of the Adsorption of Rhodamine 6G on Laponite B for Low Loadings. *Clay Miner.* **1994**, *29*, 105–113.
35. Cummins, H. Z. Liquid, Glass, Gel: The Phases of Colloidal Laponite. *J. Non-Cryst. Solids* **2007**, *353*, 3891–3905.
36. Lutkenhaus, J. L.; Olivetti, E. A.; Verploegen, E. A.; Cord, B. M.; Sadoway, D. R.; Hammond, P. T. Anisotropic Structure and Transport in Self-Assembled Layered Polymer−Clay Nanocomposites. *Langmuir* **2007**, *23*, 8515–8521.
37. Rouse, J. H.; MacNeill, B. A.; Ferguson, G. S. Sol-Gel Processing of Ordered Multilayers to Produce Composite Films of Controlled Thickness. *Chem. Mater.* **2000**, *12*, 2502–2507.
38. Bond, S. P.; Hall, C. E.; McNerlin, C. J.; McWhinnie, W. R.; Walton, D. J. Coordination-Compounds on the Surface of Laponite-Tri-2-Pyridylamine Complexes. *J. Mater. Chem.* **1992**, *2*, 37–41.
39. Giannakopoulos, E.; Stathi, P.; Dimos, K.; Gournis, D.; Sanakis, Y.; Deligiannakis, Y. Adsorption and Radical Stabilization of Humic-Acid Analogues and Pb^{2+} on Restricted Phyllomorphous Clay. *Langmuir* **2006**, *22*, 6863–6873.
40. Xue, W.; He, H.; Zhu, J.; Yuan, P. FTIR Investigation of CTAB-Al-Montmorillonite Complexes. *Spectrochim. Acta* **2007**, *A67*, 1030–1036.
41. Mahadevaiah, N.; Venkataramani, B.; Jai Prakash, B. S. Restrictive Entry of Aqueous Molybdate Species into Surfactant Modified Montmorillonite—A Breakthrough Curve Study. *Chem. Mater.* **2007**, *19*, 4606–4612.
42. Ogawa, M.; Ishikawa, A. Controlled Microstructures of Amphiphilic Cationic Azobenzene−Montmorillonite Intercalation Compounds. *J. Mater. Chem.* **1998**, *8*, 463–467.
43. Czímerová, A.; Bujdák, J.; Dohrmann, R. Traditional and Novel Methods for Estimating the Layer Charge of Smectites. *Appl. Clay Sci.* **2006**, *34*, 2–13.
44. Acosta, E. J.; Deng, Y.; White, G. N.; Dixon, J. B.; McInnes, K. J.; Senseman, S. A.; Frantzen, A. S.; Simanek, E. E. Dendritic Surfactants Show Evidence for Frustrated Intercalation: A New Organoclay Morphology. *Chem. Mater.* **2003**, *15*, 2903–2909.